The carbonate concentration mechanism of *Pyropia yezoensis* (Rhodophyta): Evidence from transcriptomics and biochemical data

Baoyu Zhang (byzhang@qdio.ac.cn)
Institute of Oceanology Chinese Academy of Sciences https://orcid.org/0000-0001-7278-0219
Xiujun Xie
Institute of Oceanology Chinese Academy of Sciences
Yuanyuan Sun
Institute of Oceanology Chinese Academy of Sciences
Guangce Wang
Institute of Oceanology Chinese Academy of Sciences

Research article

Keywords: Carbon concentrating mechanism, enzyme activity, Pyropia yezoensis, photosynthetic efficiency, transcriptome

Posted Date: March 9th, 2020

DOI: https://doi.org/10.21203/rs.3.rs-16280/v1

Version of Record: A version of this preprint was published at BMC Plant Biology on September 15th, 2020. See the published version at https://doi.org/10.1186/s12870-020-02629-4.

Abstract

Background *Pyropia yezoensis* (Rhodophyta) is widely cultivated in East Asia and plays important economic, ecological and research roles. Although inorganic carbon utilization of *P. yezoensis* has been researched from a physiological aspect, the carbon concentration mechanism (CCM) of *P. yezoensis* remains unclear. To explore the CCM of *P. yezoensis*, especially during its different life stages, we tracked changes in the transcriptome, photosynthetic efficiency and in key enzyme activities under different inorganic carbon concentrations.

Results Photosynthesis efficiency demonstrated that sporophytes were more sensitive to low carbon (LC) than gametophytes, with increased photosynthesis during both life stages under high carbon (HC) compared to normal carbon (NC) conditions. The structures of pyrenoids and starch and lipid droplets in cells corresponded with their growth reaction to different inorganic carbon (Ci) concentrations. We constructed 18 cDNA libraries from 18 samples (three biological replicates per Ci treatment at two life cycles stages) and sequenced these using the Illumina platform. De novo assembly generated 182,564 unigenes, including approximately 275 unigenes related to CCM. Most genes encoding internal carbonic anhydrase (CA) and bicarbonate transporters (anion exchange protein and ATP-binding cassette (ABC) transporter) involved in the biophysical CCM pathway were induced under LC in comparison with NC, with transcript abundance of these PyCA s in gametophytes typically higher than that in sporophytes. We identified all key genes participating in the C4 pathway and showed that their RNA abundances changed with varying Ci conditions. In particular, phosphoenolpyruvate carboxylase (PEPC) transcript abundance was significantly induced under LC conditions. Activities of key enzymes involved in the C4-like pathway were higher under HC than under the other two conditions, with enzyme activities slightly higher in sporophytes than in gametophytes, except for phosphoenolpyruvate carboxykinase (PEPCK).

Conclusion We elucidated the CCM of *P. yezoensis* from transcriptome and enzyme activity levels. All results indicated at least two types of CCM in *P. yezoensis* , one involving CA and an anion exchanger (transporter), and a second, C4-like pathway belonging to the PEPCK subtype, possibly located in mitochondria. The latter pathway plays roles in both the sporophyte and gametophyte life cycles.

Background

Seaweeds are important marine photoautotrophs, playing an important part in global primary production and carbon sequestration [1, 2, 3].

Ocean water contains about 90% inorganic carbon, mainly in the form of HCO_3^- with the remainder as carbonate ions (CO_3^{2-}) and dissolved CO_2 [4]. Due to the low amount of CO_2 in seawater, most macroalgae have evolved a carbon concentrating mechanism (CCM) to utilize HCO_3^- for maintaining high levels of growth [5, 6, 7]; these CCMs are increasingly important because rising CO_2 in the air has led to rising levels of HCO_3^- in water over the past few decades [8, 9]. Despite the ecological, economic and cultural importance of macroalgae, we know relatively little about their CCMs.

Various types of CCMs have been discovered in terrestrial plants and microalgae: biophysical, biochemical and basal CCM, respectively. Biophysical CCMs involve carbonic anhydrase (CA) and bicarbonate transporters. A biochemical CCM is also called the C4-like pathway. Three subtypes of C4 photosynthesis are recognized, based on the principal decarboxylating enzyme used in the bundle sheath: NADP-malic enzyme (NADP-ME), NAD-malic enzyme (NAD-ME) and phosphoenolpyruvate carboxykinase (PEPCK) [10]. In basal CCMs, mitochondrial γ-CAs and NADH–ubiquinone oxidoreductase complex I of the respiratory chain recycle mitochondrial CO_2 for carbon fixation in chloroplasts and thus reduce leakage of CO_2 from plant cells [11, 12].

Species of the genus Pyropia belong to the Rhodophyta are among the most economically important macroalgae in East Asia, including China, Japan and South Korea. The Pyropia life cycle involves a macroscopic leafy thallus phase (gametophyte) alternating with a microscopic filamentous thallus phase (sporophyte). Because of its great economical, ecological, nutritional and research value, Pyropia has been recognized as a model seaweed among marine plants [13, 14].

Extensive surveys have explored the physical reaction of Pyropia to rising CO_2, indicating that elevated CO_2 concentration (1000–1200 ppm) can enhance growth of Pyropia yezoensis [15, 16]; moreover, inorganic carbon (Ci) uptake styles differ between sporophytes and gametophytes. For instance, Yue et al. and Li et al. reported that gametophytes of P. yezoensis utilize HCO_3^- via extracellular carbonate anhydrase (eCA), but exhibit weak ability to directly use HCO_3^- [17, 5]. Luo et al. indicated that sporophytes absorb Ci through active transport of HCO_3^- and CO_2 [18]. By contrast, data from Expressed Sequence Tag (EST) and transcriptome studies suggest the possible existence of a C4-like pathway in P. yezoensis and Pyropia haitanensis, but whether this functions in P. yezoensis remains unknown [19, 20, 21].

To explore CCMs in P. yezoensis, we cultivated gametophytes and sporophytes under three different Ci conditions by adjusting the amount of $NaHCO_3$ in artificial seawater. We tracked their growth, transcriptome and relative enzyme activities under different Ci conditions. Our results provide explanations for the divergence of CCMs between the two life stages of P. yezoensis.

Results

Illumina sequencing, de novo assembly and annotation

To explore the CCM of P. yezoensis, we cultivated gametophytes and sporophytes under different Ci conditions and constructed 18 cDNA libraries (generated from three biological replicates of the two life stages under the three treatments). Using Illumina Hiseq sequencing technology, each reaction can yield 2 × 150 bp independent reads from either end of a DNA fragment. We obtained high-quality clean reads accounting for more than 97.83% of the raw reads (Additional file1, Table S1).

After assembling the high-quality clean reads from the high-throughput sequencing data, 182,564 unigenes were identified with a contig N50 size of 945 bp and average unigene size of 837 bp (Table 1). The length of these assembled unigenes ranged from 200 to 42,138 bp. Unigenes with lengths between 401 and 600 bp were predominant, comprising approximately 36.54% of the total number of unigenes; the next most abundant size class was 601–1000 bp, constituting 27% of the total unigenes (Additional file 2, Fig. S1). We performed BLAST analysis on all 182,564 unigenes using the following databases: NCBI non-redundant protein sequences (Nr), Swiss-Prot, Kyoto Encyclopedia of Genes and Genomes database (KEGG), and Clusters of Orthologous Groups of proteins (COG). We found 59,825 (32.77%), 59,327 (32.49%) and 53,110 (32.5%) unigenes in Swiss-Prot, Nr, and KEGG, respectively (Additional file3, Table S2). All these data indicated that the RNA-seq data met the quality standard for further analysis. After primary analysis, we identified around 275 unigenes related to CCM pathways.

Table 1
summary of Trinity assembly of the RNA-seq data
of P. yezoensis

Total unigenes num.:	**182564**
Total unigenes length:	152921448
Total isoform num.	202495
Total isoform length	181907159
Average Unigene length:	837.631997546066
Largest unigene:	42138
N50:	945

Physiological responses and change of pH under different Ci conditions

We tracked the pH of water and physiological characteristics of the two different life cycle stages under different Ci culturing conditions.

In sporophytes, pH ranged from 8.03 ± 0.03 to 8.64 and 8.59 ± 0.03 under high carbon (HC) and normal carbon (NC) conditions, respectively. Under low carbon (LC), pH ranged from 8.00 ± 0.03 to 8.32 ± 0.03 (Fig. 1). Sporophyte growth slowed down under LC, yet remained vigorous under HC. Under LC, photosynthetic efficiency was around 18.75% lower than that under NC, while it was enhanced by about 14.19% under HC compared with NC, as indicated by changes in photosystem II (YII) (Fig. 2).

In gametophytes, the pH ranged from 8.04 ± 0.02 to 8.78 ± 0.03 under HC, from 8.02 ± 0.02 to 8.65 ± 0.04 under NC and from 8.02 ± 0.03 to 8.4 ± 0.02 under LC (Fig. 1). Photosynthetic efficiency was almost 6.8%

lower under LC than under NC, while it was enhanced by 16.87% under HC compared with that under NC (Fig. 2).

Induction of bicarbonate transporters and CA under different Ci indicates the presence of a biophysical CCM

In this transcriptome, three CA unigenes, DN38784_c0_g1, DN 99529_c0_g1 and DN105005_c0_g1, predicted to be located in the chloroplast or thylakoid lumen by TargetP software, were upregulated under LC compared with NC. Transcripts of DN105005_c0_g1 increased by 2.08- and 1.1-loget in gametophytes and sporophytes under LC compared with NC, respectively. Moreover, for DN38784_c0_g1, DN 99529_c0_g1 and DN50495 _c0_g1, the latter also predicted to be located in the thylakoid lumen, expression in gametophytes was significantly higher than that in sporophytes under the three Ci conditions. Such induction of specific CAs by low HCO_3^- stress suggests an active biophysical CCM. In addition, other CA unigenes (DN120854_c0_g1, DN59301_c0_g1), predicted to be located in the periplasm, showed very low reads per kilobase of exon model per million mapped reads (RPKM) values in sporophytes and showed higher expression levels under HC compared with NC.

Anion exchange proteins and ABC-transporters may play the role of bicarbonate transporter, as indicated from the transcriptome. Expression of DN101765_c1_g1, a putative Band 3 anion transporter sharing 58% amino acid sequence identity with its known counterparts from Porphyridium purpureum (KAA8497371) and Gracilariopsis chorda (PXF50105), was increased by 0.4- and 0.5-loget in sporophytes and gametophytes, respectively, under LC compared with NC. Expression of a putative anion exchange protein, DN107803_c0_g1, was increased 0.36- and 0.65-loget in sporophytes and gametophytes, respectively, under LC compared with NC. These two transporters showed no obvious difference under HC conditions compared with NC. In addition, transcripts of several ABC-transporters (105272_c0_g1, 109304_c3_g1) were upregulated under LC compared with NC in the two life cycles; moreover, the RPKM values of these unigenes in sporophytes were significantly higher than those in gametophytes.

Increased transcript abundance and enzyme activity of C4-like enzymes under different Ci indicates an active biochemical CCM

Key genes involved in the C4-pathway were all identified in this transcriptome. BlastX search showed that DN107354_c0_g1 had 100% amino acid sequence identity with PEPC in P. yezoensis (accession no. AIT70077) and was predicted to be located in mitochondria (Additional file 4, Table S4). It was induced by LC and increased 0.44- and 0.34-loget compared with NC conditions in gametophytes and sporophytes, respectively, but was downregulated under HC. Its enzyme activity under HC was 119.3 and 103.9 nmol/min/g FW in sporophytes and gametophytes, respectively, higher than under LC and NC conditions (Fig. 3). We identified DN101889_c0_g3 and DN101912_c0_g1 as transcripts of PEPCK due to

very high amino acid identity (64–77%), and predicted them to be targeted to mitochondria. These two transcripts were induced by 0.53- and 1.45-loget, respectively, under HC compared with NC in sporophytes. However, the RPKM values of these two unigenes in gametophytes were zero. Despite the relatively low transcript level, PEPCK showed very high enzyme activity in the two life cycles, even above 5400 nmol/min/g FW (Fig. 3). The enzyme activity of PEPCK under HC in gametophytes was a little higher than that in sporophytes, 6076.2 and 6238.7 nmol/min/g FW, respectively. DN141134_c0_g1, DN14534_c0_g1, DN87488_c0_g1 and DN49711_c0_g1 were identified as putative unigenes of pyruvate phosphate dikinase (PPDK); their abundance was commonly low in sporophytes, and RPKM values were almost zero in gametophytes. DN141134_c0_g1, DN14534_c0_g1 and DN49711_c0_g1 were induced under LC compared with NC in sporophytes, while DN14534_c0_g1, DN87488_c0_g1 and DN49711_c0_g1 were also induced by HC. Enzyme activity of PPDK under HC was higher than that under LC and NC. Moreover, the enzyme activity of PPDK in sporophytes was about one fold higher that of gametophytes. DN34191_c0_g1 and DN50799_c0_g1 encode NAD-malate dehydrogenase (MDH), and we predicted that they are targeted to the mitochondria and chloroplast, respectively (Additional file4, Table S3). They were induced under LC compared with NC but there was no obvious divergence in expression levels between LC and NC conditions in sporophytes. However, levels of the unigene DN50799_c0_g1 increased 1.08-loget under LC compared with NC in gametophytes. The enzyme activity of NAD-MDH in sporophytes was commonly higher than that in gametophytes and was usually higher under HC relative to LC and NC: 835.6 and 688.5 nmol/min/g FW in sporophytes and gametophytes under HC, respectively (Fig. 3)

Although we identified a few unigenes encoding ME, their expression level was either very low or showed no obvious difference under different Ci concentrations. Enzyme activity of NADP-ME in sporophytes was higher than that in gametophytes, at 347.7 and 293.3 nmol/min/g FW under HC, respectively (Fig. 3).

Among the five key enzymes involved in the C4-pathway, the highest enzyme activity was observed among PEPCKs, and the lowest activity was for PEPCs. The activity of NAD-MDH was commonly higher than that of NADP-ME.

Transmission electron microscopy (TEM) observation of cells from the two life stages under three Ci conditions

Both gametophytes and sporophytes of P. yezoensis exhibited significant changes in lipids and starches, and even pyrenoid structure, with changing environmental conditions (Fig. 4). After being cultured for 54 hs under LC, starches were undetectable in cells of both gametophytes and sporophytes, and there were more lipid droplets in cells of gametophytes than those of sporophytes. Under HC, cells of the two life stages had dramatically more starches than cells growing under NC, usually distributed between chloroplasts in sporophytes but outside of chloroplasts in gametophytes. Under NC, we observed a small amount of starches in the cells of sporophytes but barely any in gametophytes. Pyrenoid structure in gametophytes was loose and there were many ribosomes spread throughout the cytoplasm, while in

sporophytes, pyrenoid structure was relatively tight and there were fewer ribosomes than in gametophytes.

Validation of RNA-seq findings with real-time fluorescent quantitative PCR (qRT-PCR)

We used qRT-PCR to detect expression levels under the three Ci conditions between the two life stages of seven target genes from different functional categories. All the genes used in this validation showed very similar expression patterns to those revealed by RNA-seq results (Fig. 5A, B), demonstrating the reliability of the RNA-seq data.

Discussion

Physical characteristics of the two life cycles under different Ci conditions

The effective photochemical quantum yield of photosystem II is directly related to the CO_2 assimilation rate and represents the photosystem II state [22, 23]. In this work, LC had more effect on sporophytes than on gametophytes, indicated by reduced photosynthetic efficiency of YII under LC conditions. Thus, pH change under LC culture was comparatively less for sporophytes relative to gametophytes. Under HC conditions, the photosynthetic efficiency of gametophytes was higher than that of sporophytes, so the pH of HC medium rose more quickly for gametophytes, accordingly. These results indicated that the reactions of sporophytes and gametophytes to the change of Ci concentration are different; sporophytes are more sensitive to the LC relative to gametophytes, while elevated Ci enhances the photosynthetic efficiency of photosystem II in gametophytes more than in sporophytes. This result was in agreement with results of TEM. When P. yezoensis was cultured under LC, starches were firstly consumed, and then lipids. There were more lipid droplets in cells of gametophytes relative to those of sporophytes, enabling gametophytes to endure the Ci deprivation for much longer and maintain growth. Since gametophytes of Pyropia have a low carbonate compensation point, 40.7 ± 11.8 μmol/L at pH 8.2, significantly lower than the natural seawater Ci concentration (about 2.21 mM) [24], their growth is not limited by Ci and they use the elevated Ci to invest in lipid storage, as shown in Fig. 4. Gametophytes showed higher photosynthetic activity than sporophytes, accumulating more starches and lipid droplets than sporophytes under abundant Ci. Huan (2018) studied the response of the photosynthetic reaction in the two life stages of P. yezoensis to increasing CO_2, and found that YII in gametophytes was enhanced as CO_2 increased; however, there were no significant differences in YII of sporophytes [25]. Wang (2019) also reported that net photosynthetic rates (Pn) of thalli gametophytes were about 2.9 times that of conchocelis sporophytes of P. haitanensis, and the maximal quantum yield of photosystem II (Fv/Fm) was significantly higher than that of the conchocelis at pH 8.0 [26]. All these results suggest that gametophytes of Pyropia have a higher growth rate than sporophytes under abundant Ci conditions.

Biophysical CCM in the two different life cycles of P. yezoensis

Facing the phenomenon of rising global CO_2, researchers are paying more attention to the inorganic carbonate utilization of macroalgae, including Pyropia. Work has been conducted to explore the physiological reaction to rising CO_2, the pH compensation point, and the physiological reaction after adding different types of inhibitors [18, 24, 27, 28]. The pH compensation point of gametophytes and sporophytes of P. haitanensis is pH 9.9 and 9.95, respectively, and of gametophytes of P. yezoensis is pH 9.65 [18, 5]. High pH compensation point corresponds to the presence of CCMs [29, 24]. However, despite the above inferences, we still lack direct molecular evidence. In this study, we found higher abundance of most iCA genes in gametophytes than in sporophytes, which indicated that biophysical CCMs play a more important role in gametophytes relative to sporophytes. This might be one of the reasons for gametophytes growing more rapidly than sporophytes.

Since HCO_3^- is not freely permeable across the lipid bilayer of biological membranes, it is either transported by membrane transporter proteins or obtained in the form of CO_2, which is then converted by periplasmic CA [30]. HCO_3^- uptake in the two different Pyropia life stages has been elucidated by physiological reactions to different types of inhibitors, such as acetazolamide (AZ), eCA inhibitor, ethoxyzolamide (EZ), iCA inhibitor and an inhibitor of the HCO_3^- transporter, 4,4'-diisothiocyanato-stilbene-2,2'-disulfonic acid (DIDS). Luo and his coworkers (2002) examined the inhibitory effect of AZ, DIDS and vanadate, an inhibitor of ATPase associated with the plasma membrane, on sporophytes of P. haitanensis. They showed inhibitory rates of 25.3% and 71.3%, respectively, after adding AZ and vanadate, and inferred that eCA is not an important part of Ci uptake in P. haitanensis conchocelis, with most Ci absorption occurring through active transport of HCO_3^- and CO_2 [18]. Later, Li and his coworkers (2016) suggested that the gametophytes of P. yezoensis show active HCO_3^- uptake by studying their reaction to enhanced CO_2 in the atmosphere [5]. Recently, Wang (2019) studied the physiological reaction to Ci utilization between gametophytes and sporophytes of P. haitanensis and found that the Pn of thallus was significantly inhibited by AZ and EZ. For conchocelis, inhibition by EZ was greater than that by AZ. Inhibition of conchocelis by DIDS was greater than that of thallus. All these results indicate that iCA and eCA play essential roles in HCO_3^- utilization in gametophytes, while iCA is more important than eCA in sporophytes. At the same time, the absorption of HCO_3^- via the DIDS-sensitive anion transport protein is less important in gametophytes than in sporophytes [26].

The results from our transcriptome data revalidated the above opinions. Unigenes encoding iCA were induced by LC; moreover, the transcript abundance of iCA genes was significantly higher in gametophytes relative to sporophytes. However, unigenes encoding eCA showed very low RNA amounts in sporophytes, and almost undetectable amounts in gametophytes. We identified some unigenes encoding anion exchange proteins and ABC-transporters, and these were upregulated under LC compared with NC. Moreover, the abundance of these genes encoding bicarbonate transporters was higher in sporophytes

relative to gametophytes. These data are in agreement with evidence from inhibitory experiments that anion exchange proteins and ABC- transporters make a great contribution to HCO_3^- transportation in sporophytes of P. yezoensis.

Bicarbonate transporters are divergent within the microalgae and macroalgae. In Macrocystis pyrifera (Phaeophyta), anion exchange protein plays the main role in bicarbonate uptake, while in microalgae, such as Nannochloropsis oceanica and Chlamydomonas reinhardtii, ABC-transporters play an essential role in HCO_3^- transportation [31, 32, 33]. In Phaeodactylum tricornutum, the solute carrier family is the HCO_3^- transporter [34].

Biochemical CCM in P. yezoensis

Besides the C3 pathway, a C4-like pathway might exist in Pyropia. Fan et al. (2007) constructed an EST library of P. haitanensis sporophytes and found abundant PEPCK ESTs; they primarily inferred that a C4-like pathway might exist in sporophytes of P. haitanensis [20]. Later, genes involved in the C4-like pathway were identified in P. yezoensis, except PPDK [19]. Xie and his coworkers (2013) obtained the transcriptomes of gametophytes and sporophytes of P. haitanensis and found some key genes involved in the C4-pathway, but no unigenes encoding PPDK or MDH. They inferred that the C4-like pathway plays a role in sporophytes, according to relative expression levels of PEPCK and PEPC [21]. In fact, there has not been enough direct evidence so far to support this opinion.

In our work, we not only found all the key genes involved in the C4-like pathway, including unigenes encoding PPDK, but we also detected the activity of these enzymes under different Ci conditions. In our work, genes encoding PEPC and NAD-MDH were all induced by LC; moreover, the abundance of PEPC transcripts in gametophytes was higher than that in sporophytes according to the transcriptome, which was verified by qRT-PCR results (Fig. 5A). Although the amounts of PEPCK unigenes and PPDK unigenes in this transcriptome were relatively low in sporophytes and gametophytes, these enzymes showed high levels of activity, especially PEPCK. All the key enzymes involved in the C4-like pathway showed high levels of activity and a similar pattern in the two life stages under HC and NC conditions, with the exception of PPDK enzyme activity.

Combining the predicted subcellular location results, we constructed an overview of the biochemical CCM of P. yezoensis (Fig. 6). We primarily suggest that the C4-like pathway might be located in the mitochondrion and belong to the PEPCK subtype, and transport concentrated CO_2 to the C3 pathway in chloroplasts. Moreover, the C4-like pathway not only plays a role in sporophytes, but also plays a role in gametophytes under NC and HC conditions, unlike the previous hypothesis. This is one of the reasons that gametophytes show higher photosynthesis levels than sporophytes.

Conclusions

The CCM in P. yezoensis includes biophysical CCM and biochemical CCM, and they play an essential role for the growth of P. yezoensis. The two CCMs perform different roles according to environmental Ci concentrations. The biophysical CCM plays a more important role in gametophytes than in sporophytes, and the C4-like pathway also plays a role under high Ci conditions, explaining why gametophytes grow faster than sporophytes. Although the two CCMs also play a role in sporophytes under normal and high Ci conditions, the biophysical CCM in gametophytes is stronger than that in sporophytes.

Materials And Methods

Algal materials

Sporophytes of P. yezoensis were obtained from our laboratory algae collection in the Institute of Oceanology, Chinese Academy of Sciences, Qingdao, China, and gametophytes of this species were generated from sporophytes under laboratory conditions. Before incubating in artificial seawater with different dissolved Ci concentrations, thallus gametophytes and filamentous sporophytes were cultured in Provasoli's enriched seawater medium at 18 °C under 12 h light:12 h dark at 30 μmol/m^2/s.

Artificial seawater (g/L: NaCl 20.758, $NaSO_4$ 3.477, $CaCl_2$ 1, KCl 0.587, $MgCl_2{\cdot}6H_2O$ 9.359, $NaHCO_3$ 0.17, KBr 00845, H_3BO_3 0.0225, NaF 0.0027, $SrCl{\cdot}6H_2O$ 0.0214) was used for NC conditions. There was no $NaHCO_3$ in artificial seawater representing LC and 4 mM HCO_3^- (0.34 g/L) in artificial seawater with HC. $NaHCO_3$ was added to the artificial seawater after autoclaving, and the pH was then adjusted to around 8.1.

Transcriptome sampling, sequencing and analysis

Gametophytes and sporophytes were cultured in the three media mentioned above (LC, NC, HC) in a Multi-cultivator MC 1000-OD (Photon Systems Instruments, Drasov, Czech Republic) with cool white light (30 μmol photons/m^2/s) at 18 °C. Fresh materials (0.05 g) were inoculated into 80 mL medium with three biological replicates for each Ci concentration. To avoid disturbance from outside carbon sources, media were bubbled continuously with mixed gas of high purity nitrogen and oxygen (4:1). After culturing for 54 h, 18 samples were collected for transcriptomic analyses. Total RNA from each sample was extracted using Trizol reagent (Invitrogen, Thermo Scientific, USA). RNA concentration and purity were determined spectrophotometrically (NanoDrop-1000, Thermo Scientific, USA). Strand-nonspecific transcriptome libraries were prepared using a TruseqTM RNA sample prep Kit (Illumina, USA) and sequenced for 2 × 150 bp runs (paired-end) using an Illumina HiSeq 2000 at Biozeron Biotech. Co. Ltd, China.

After sequencing, the raw reads datasets were evaluated using Trimmomatic software (http://www.usadellab.org/cms/uploads/supplementary/Trimmomatic). Adapter sequences and lower-quality reads (shorter than 30 bp or quality score lower than 20) were filtered to obtain high-quality mRNA sequencing reads (Additional file 1, Table S1). The high-quality reads from all samples were merged for de novo assembly using Trinity software V2.2.0 (http://trinityrnaseq.sourceforge.net/) to produce an

assembly gene set. All of the raw reads generated in this study have been deposited in CNSA (https://db.cngb.org/cnsa/) of CNGBsb with accession code CNP0000880.

The assembled gene set was used for BLASTX search (BLAST + 2.7.1, E Value ≤ 1e-5) against the NR, Swiss-prot and KEGG databases for functional annotation. Gene expression under each experimental condition was measured as the number of aligned reads to annotated genes determined by Cufflinks (version 2.0.4) and normalized to RPKM values.

Measurements of photosynthetic parameters and pH

pH, chlorophyll fluorescence of PSII (YII), maximum quantum yield (Fv/Fm), and dissolved CO_2 and O_2 concentrations were detected in real time in a flat-panel photobioreactor (Photobioreactor FMT 150 from Photon System Instruments). Culturing conditions were the same as those of the Multi-cultivator MC 1000-OD bioreactor, with 0.4 g fresh weight (FW) of P. yezoensis gametophytes or sporophytes added to 800 mL medium. Two biological replicates were conducted.

Validation of transcript abundance using qRT-PCR

To further test the validity of the mRNA-Seq results, total RNA extracted from the same cultures was used for cDNA synthesis with a PrimeScript® RT reagent Kit with gDNA Eraser (Takara, Japan). qRT-PCR was performed by standard methods (Roche, Switzerland) as described previously [35], with Eukaryotic initiation factor 4A (EIF4A, TRINITY_DN83248_c0_g1) as an internal reference gene. Ct values were determined for triplicate independent technical experiments performed on triplicate biological cultures (n = 3). Primer pairs used for qRT-PCR analyses are listed in Additional file 4, Table S3.

Predicting the subcellular localization of proteins

To determine possible compartmentalization of CCMs, two programs, SignalP and TargetP, were used to predict subcellular localization. The SignalP 5.0 server (http://www.cbs.dtu.dk/services/SignalP/) predicts the presence of signal peptides and the location of their cleavage sites in proteins from Archaea, Bacteria and Eukarya. The TargetP-2.0 server (http://www.cbs.dtu.dk/services/TargetP/) predicts the presence of N-terminal presequences: signal peptide, mitochondrial transit peptide, chloroplast transit peptide or thylakoid luminal transit peptide. Results from the two programs were pooled, and locations with higher scores were chosen as the predicted localization for a particular protein. Unigenes encoding the key enzymes involved in the biochemical CCM pathway are listed in Additional file 5, Table S4.

Measurement of the enzymatic activity of proteins encoded by C4-like pathway genes

Enzymatic activities of PEPC, PEPCK, PPDK, NADP-ME and NAD-MDH were measured using quantification kits (Keming Biotech, China). About 100 mg fresh algal materials were ground on ice, and 1 mL extraction buffer from the respective kit was added. The mixture was stirred to homogeneity and centrifuged at 4 °C, 10,000 g for 10 min. Supernatants were incubated on ice for further enzyme assays. Enzyme activities were determined spectrophotometrically using a UV-1800 spectrophotometer by

measuring at 340 nm in total volumes of 0.2 mL and in triplicate. Change in absorbance was recorded for 5 min. The activity of different enzymes was calculated based on the content of fresh algal materials (mg), with the activity unit defined as nmol NAD(P)H oxidation or NAD(P) + reduced per minute per gram fresh weight.

Transmission Electron Microscopy

Samples were collected in a centrifuge tube after being cultivated for 54 h. Samples were then fixed in a solution of 4% glutaraldehyde with 0.01 M phosphate buffer, pH 7.4, at 4 °C and then centrifuged for 10 min, 5000 g at room temperature. Pellets were washed with phosphate buffer, and then post-fixed with 1% osmium tetroxide (Ted Pella INC, California, USA) in phosphate buffer, pH 7.4, for 1.5 h before washing three times with 0.01 M phosphate buffer at 4 °C. The samples were dehydrated in a series of ethanol from 30%-100%, infiltrated with acetone (Tieta, Laiyang, China) and epoxy resin (SPI – CHEM, USA) mixture, and embedded and polymerized in epoxy resin. Sections were cut with a Leica EM UC7 ultramicrotome (Leica Microsystems, Germany), stained with citrate and examined with a transmission electron microscope (HT7700, Hitachi, Tokyo, Japan).

Abbreviations

ABC transporter: ATP-binding cassette transporter; AZ: acetazolamide; CA: carbonic anhydrase; eCA: extracellular carbonate anhydrase; EST: expressed sequence tag; CCM: carbon concentration mechanism; iCA: internal CA; Ci: inorganic carbon; HC: high carbon; LC: low carbon; MDH: malate dehydrogenase; ME: malic enzyme; NC: normal carbon; PEPC: phosphoenolpyruvate carboxylase; PEPCK: phosphoenolpyruvate carboxykinase; PPDK: pyruvate phosphate dikinase; RPKM: reads Per kilobase of exon model per million mapped reads; TEM: transmission electron microscopy.

Declarations

Acknowledgements

We are grateful to Dr. Wei Zhou (Marine Fisheries Institute of Jiangsu, Nantong, China) for generously offering us *P. yezoensis* materials for many years, and we also thank International Science Editing (http://www.internationalscienceediting.com) for editing this manuscript.

Funding

This work was supported by National Natural Science Foundation of China (41876160,41876163), National key R&D program of China (2016YFC1400602-03), Key R&D program of Yantai Province (2018SFBF069).

Availability of data and materials

All of the datasets supporting the results of this article are included within the article and its additional files.

Authors' contributions

BZ conceived, designed research and analysed the transcriptome data; LH cultivated the materials and measured the enzymes. XX did the physiological experiment and made Tables. YS did the TEM sections and observed them. GW discussed the results and revised the manuscript. All authors read and approved the final manuscript.

Ethics approval and consent to participate

Not applicable

Consent for publication

Not applicable

Competing interests

The authors declare that they have no competing interests.

References

1. Gao K, McKinley KR. Use of macroalgae for marine biomass production and CO_2 remediation: a review. J Appl Phycol. 1994; 6:45–60.
2. Muraoka D. Seaweed resources as a source of carbon fixation. Bull Fish Res Agen Supplement. 2004; 1:59–63.
3. Chung IK, Beardall J, Mehta S, Sahoo D, Stojkovic S. Using marine macroalgae for carbon sequestration: A critical appraisal. J Appl Phycol. 2011; 23:877–
4. Millero FJ. Chemical Oceanography [M]. 4th Ed. Boca Raton: CRC Press, 2013, 259-333.
5. Li XH, Xu JT, He PM. Comparative research on inorganic carbon acquisition by the macroalgae Ulva prolifera (Chlorophyta) and *Pyropia yezoensis* (Rhodophyta). J Appl Phycol. 2016; 28:491–497.
6. Kevekordes K, Holland D, Haubner N, Jenkins S, Koss R, Roberts S, Raven, JA, Scrimgeour CM. et al. Inorganic carbon acquisition by eight species of Caulerpa (Caulerpaceae, Chlorophyta). Phycologia. 2006; 45(4):442-449
7. Chen BB, Lin LD, Ma ZL, Zhang TT, Chen WZ, Zou DH. Carbon and nitrogen accumulation and interspecific competition in two algae species, *Pyropia haitanensis* and *Ulva lactuca*, under ocean acidification conditions Aquacult Int. 2019; 27:721–733.
8. Wu HX, Zou DH, Gao KS. Impacts of increased atmospheric CO_2 concentration on photosynthesis and growth of micro-and macro-algae. Sci. China Ser. C Life Sci. 2008; 51:1144–1150.

9. Hepburn CD, Pritchard DW, Cornwall CE, McLeod RJ, Beardall J, Raven JA, Hurd CL. Diversity of carbon use strategies in a kelp forest community: Implications for a high CO_2 Glob. Chang. Biol. 2011;17: 2488–2497.
10. Kanai R, Edwards EG. The biochemistry of C4 photosynthesis. 1999;121: 49–87.
11. Huertas E, Colman B, Espie GS. Mitochondrial-Driven Bicarbonate Transport Supports Photosynthesis in a Marine Microalga. Plant Physiol. 2002; 130: 284–291
12. Klodmann J, Sunderhaus S, Nimtz M, Jansch L, Braun HP. Internal architecture of mitochondrial complex I from *Arabidopsis thaliana*. Plant Cell. 2010;22(3):797–810.
13. Kitade Y, Taguchi G, Shin JA, Saga N. Porphyra monospore system (Bangiales, Rhodophyta): a model for the developmental biology of marine plants. Phycol. Res. 1998; 46:17–20.
14. Saga N, Kitade Y. *Porphyra*: a model plant in marine sciences, Fish. Sci. 2002; 68 (Suppl.):1075–1078.
15. Bao ML, Wang JH, Xu TP, Wu HL, Li XS, Xu JT. Rising CO2 levels alter the responses of the red macroalga *Pyropia yezoensis* under light stress. Aquaculture. 2019; 501:325–330.
16. Gao K, Aruga Y, Asada K, Ishihara T, Akano T, Kiyohara M. Enhanced growth of the red alga *Porphyra yezoensis*Ueda in high CO2concentrations. J Appl Phycol 1991;3: 355–362.
17. Yue GF, and Zhou BC. Inorganic carbonate utilization by *Porphyra yezoensis* ueda oceanologia et limnologia sinica. 2000; 31(3):246-251 (English Abstract)
18. Luo QJ, Pei LQ, Pan SY, Wang Y, Fei ZQ. Utilization of inorganic carbon in free-living conchocelis of *Porphyra haitanensis*. Journal of Fisheries of China. 2002; 26(5):477-480.
19. Yang H, Mao YX, Kong FN, Yang GP, Wang L. Profiling of the transcriptome of *Porphyra yezoensis* with Solexa sequencing technology. Chin Sci Bull. 2011; 56(20) 2119-2130
20. Fan XL, Fang YJ, Hu SN, Wang GC. Generation and analysis of 5318 expressed sequence tags from the filamentous sporophyte of *Porphyra haitanensis* (Rhodophyta). J. Phycol. 2007; 43:1287–1294.
21. Xie CT, Li B, Xu Y, Ji DH and Chen CS. Characterization of the global transcriptome for *Pyropia haitanensis* (Bangiales, Rhodophyta) and development of cSSR markers. BMC Genomics. 2013; 14:107 http://www.biomedcentral.com/1471-2164/14/107
22. Krall JP and Edwards GE. Relationship between photosystem II activity and CO_2 fixation in leaves. Physiol Plant. 1992; 86:180–187.
23. Genty B, Harbinson J, Briantais JM and Baker NR. The relationship between photochemical quenching of chlorophyll fluorescence and the rate of photosystem II photochemistry in leaves. Photosynth. Res.1990; 25: 249–57.
24. Zou DH, Gao KS. Photosynthetic bicarbonate utilization in *Porphyra haitanensis* (Bangiales, Rhodophyta). Chin Sci Bull. 2002; 47:1629–
25. Huan L, Wang C, He LW, Lu XP, Wang XL, Liu XH, Wang GC. Preliminary comparison of atmospheric CO_2 enhancement to photosynthesis of *Pyropia yezoensis* (Bangiales, Rhodophyta) leafy thalli and filamentous thalli. Phycol Res. 2018; 66:117-126.

26. Wang YY, Wang WL, Xu Y, Ji DH, Chen CS. Physiological differences in photosynthetic inorganic carbon utilization between gametophytes and sporophytes of the economically important red algae *Pyropia haitanensis*. Algal Research. 2019; 39: 101436 https://doi.org/10.1016/j.algal.2019.101436
27. Xu K, Chen HZ, Wang WL, Xu Y, Ji DH, Chen CS, Xie CT. Responses of photosynthesis and CO_2 concentrating mechanisms of marine crop Pyropia haitanensis thalli to large pH variations at different time scales. Algal Research. 2017; 28:200–210.
28. Wang SG, Yang Y, Zhou XQ, Song DD, Xue S, Luo QJ. utilization of inorganic carbon in Pyropia haitanensis (rhodophyta) under heat stress. Oceanologia et Limnologia Sinica. 2013; 44(5):1378-1385.
29. Maberly SC. Exogenous sources of inorganic carbon for photosynthesis by marine macroalgae. J. Phycol. 1990; 26: 439
30. Poschenrieder C, Fernández JA, Rubio L, Pérez L, et al. Transport and Use of Bicarbonate in Plants: Current Knowledge and Challenges Ahead. Int J Mol Sci. 2018; 19, 1352, doi:10.3390/ijms19051352
31. Fernández PA, Hurd CL, Roleda MY. Bicarbonate uptake via an anion exchange protein is the main mechanism of inorganic carbon acquisition by the giant kelp *Macrocystis pyrifera* (Laminariales, Phaeophyceae) under variable pH. J. Phycol. 2014; 50: 998–100.
32. Wang Y, Spalding MJ. Acclimation to very low CO2: Contribution of limiting CO2 inducible proteins, LCIb and LCIA, to inorganic carbon uptake in Chlamydomonas reinhardtii. Plant Physiol. 2014; 166:2040–2050.
33. Wei L, Hajjami M E, Shen C, You WX, Lu YD, Li J. et al. Transcriptomic and proteomic responses to very low CO_2 suggest multiple carbon concentrating mechanisms in *Nannochloropsis oceanica*. Biotechnol Biofuel. 2019; 12:168, https://doi.org/10.1186/s13068-019-1506-8
34. Nakajima K, Tanaka A, Matsuda Y. SLC4 family transporters in a marine diatom directly pump bicarbonate from seawater. Proc Natl Acad Sci U S A. 2013; 110(5):1767-1772
35. Zhang BY, Yang F, Wang GC, Peng G. Cloning and quantitative analysis of the carbonic anhydrase gene from *Porphyra yezoensis* J Phycol. 2010; 46: 290-296

Additional Files

Additional file 1: Table S1. Statistics of quality control on RNA-seq data of gametophytes and sporophytes samples of *P. yezoensis* under different Ci conditions.

Additional file 2: Fig. S1. Sequence length distribution of transcriptome.

Additional file 3: Table S2. Summary of *P. yezoensis* transcriptome.

Additional file 4: Table S3. Primers used for qRT-PCR

Additional file 5: Table S4. Summary of the predicted results of some unigenes which encoding the key enzymes involved in C4-like pathway in *P.yezoensis*.

Figures

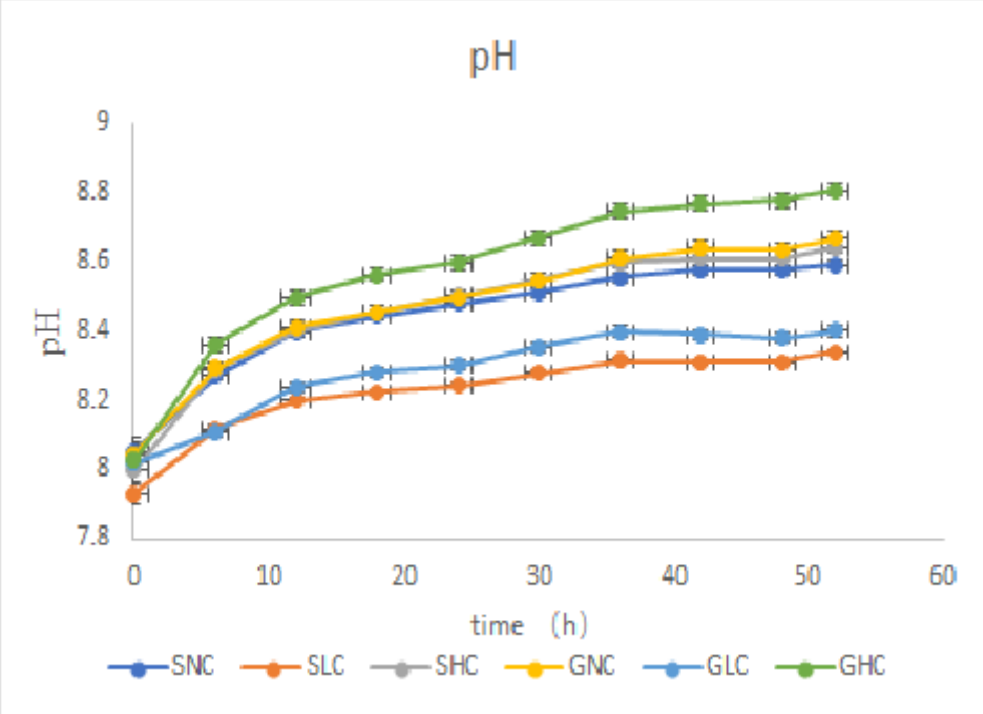

Figure 1

pH change of gametophytes and sporophytes of P. yezoensis under different Ci conditions. SNC, SHC and SLC indicate sporophytes cultivated under NC, HC and LC conditions, respectively. GNC, GHC and GLC indicate gametophytes cultivated under NC, HC and LC conditions, respectively. The results were represented by mean ± standard deviation.

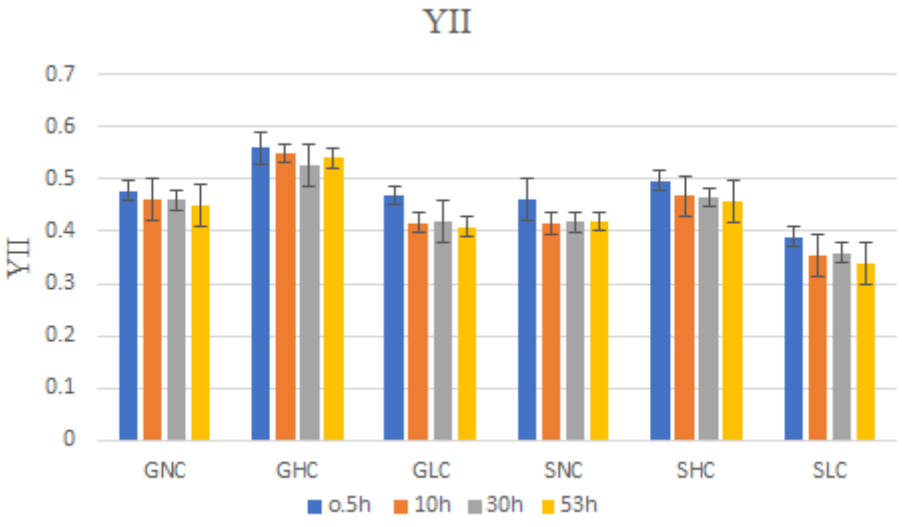

Figure 2

Variation of P. yezoensis gametophytes and sporophytes photosystem II (YII) under different Ci conditions. What the SNC, SLC, SHC, GNC, GLC and GHC represent is same as above. The results were represented by mean ± standard deviation.

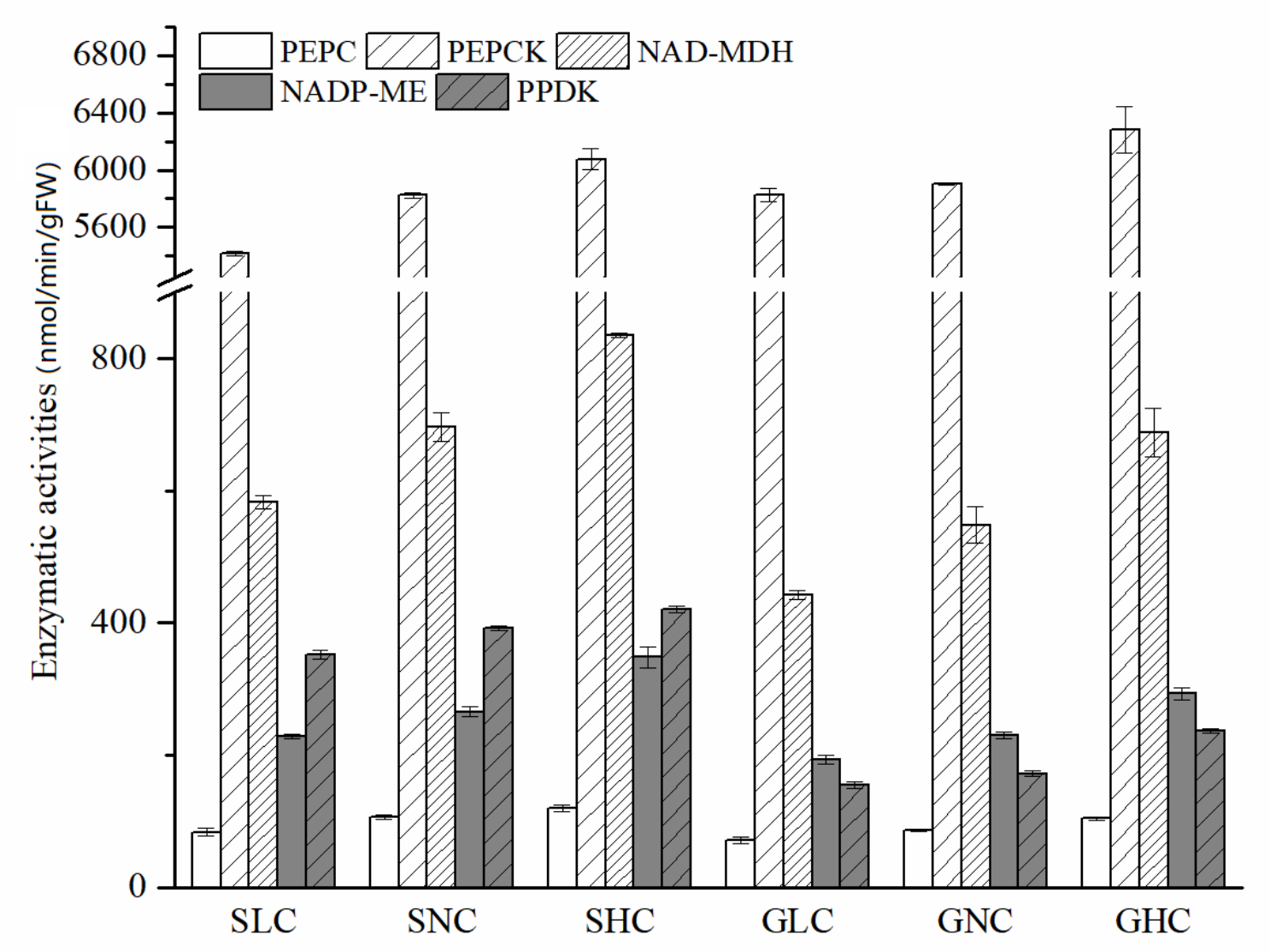

Figure 3

Activities of key enzymes involved in the biochemical pathway in the gametophytes and sporophytes of P. yezoensis under different Ci conditions. What the SNC, SLC, SHC, GNC, GLC and GHC represent is same as above. The results were represented by mean ± standard deviation.

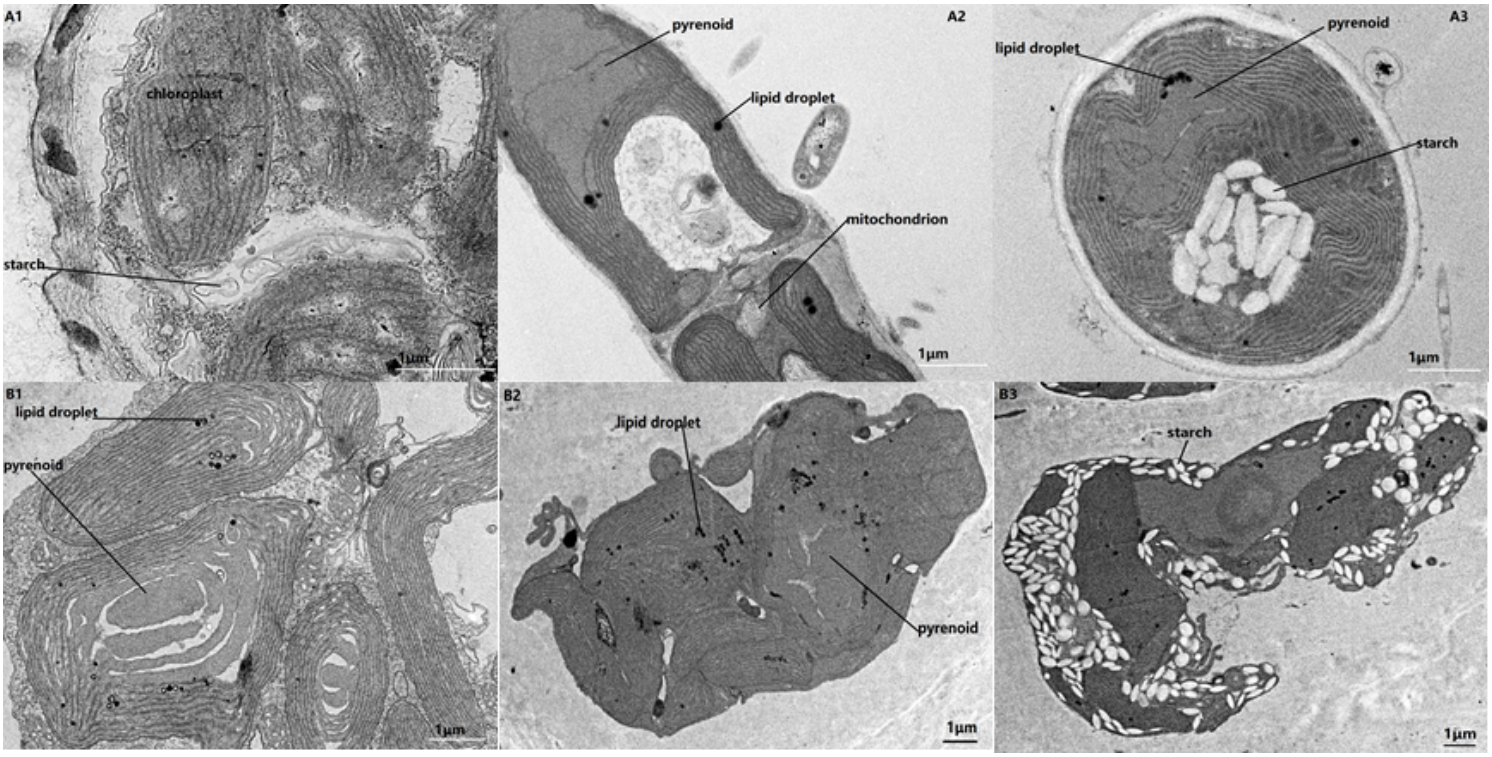

Figure 4

Transmission electron microscope imagines of sporophyte (A) and gametophyte (B) cells of P. yezoensis under three Ci conditions. Sporophytes cultivated under NC (A1), LC (A2) and HC (A3); gametophytes cultivated under NC (B1), LC (B2) and HC (B3).

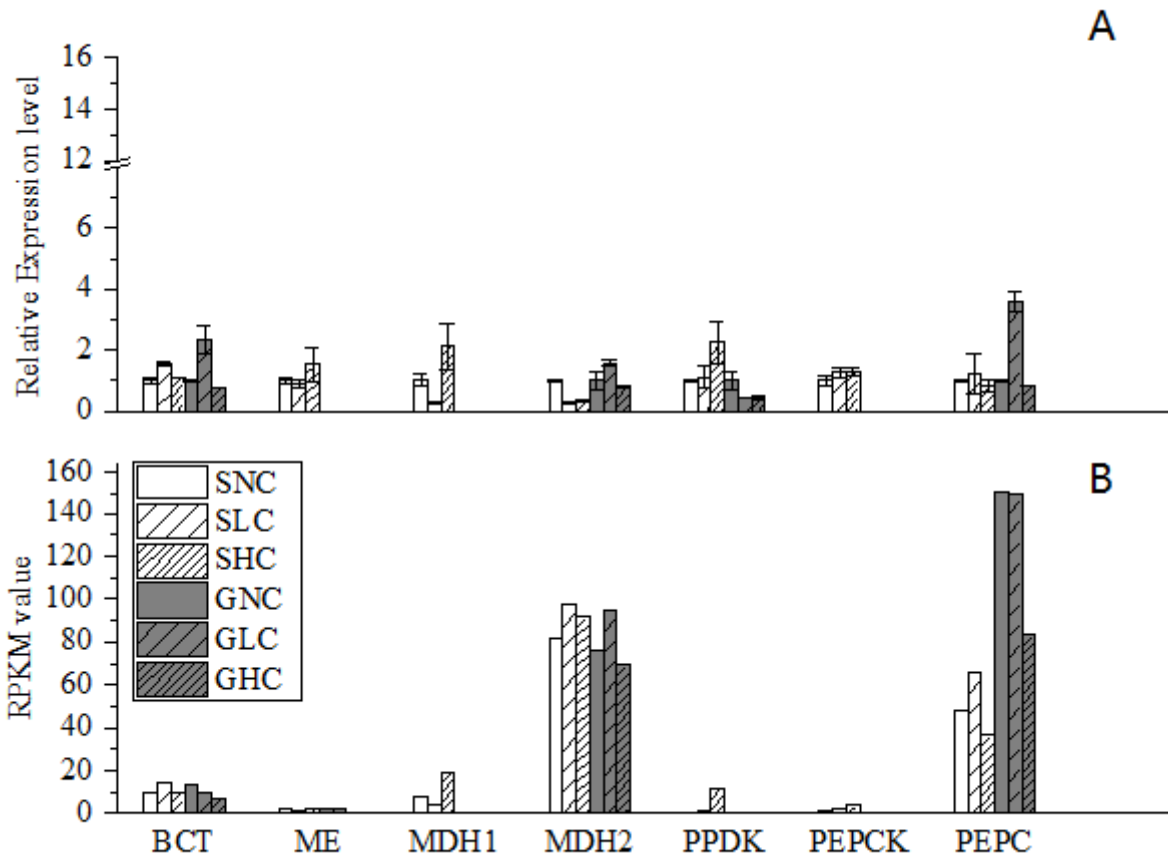

Figure 5

Gene expression for validation in (A) qRT-PCR and (B) RNA-seq assays in gametophytes and sporophytes of P. yezoensis under three Ci conditions. Data represent the mean ± standard deviation from three biological replicates. BCT (101765_c1_g1), MDH1 (DN74954_c0_g1), MDH2 (DN34191_c0_g1), PPDK (DN14534 _c0_g1), PEPCK (DN101889_c0_g1), PEPC (DN107354_c0_g1), ME (DN53078_c0_g1).

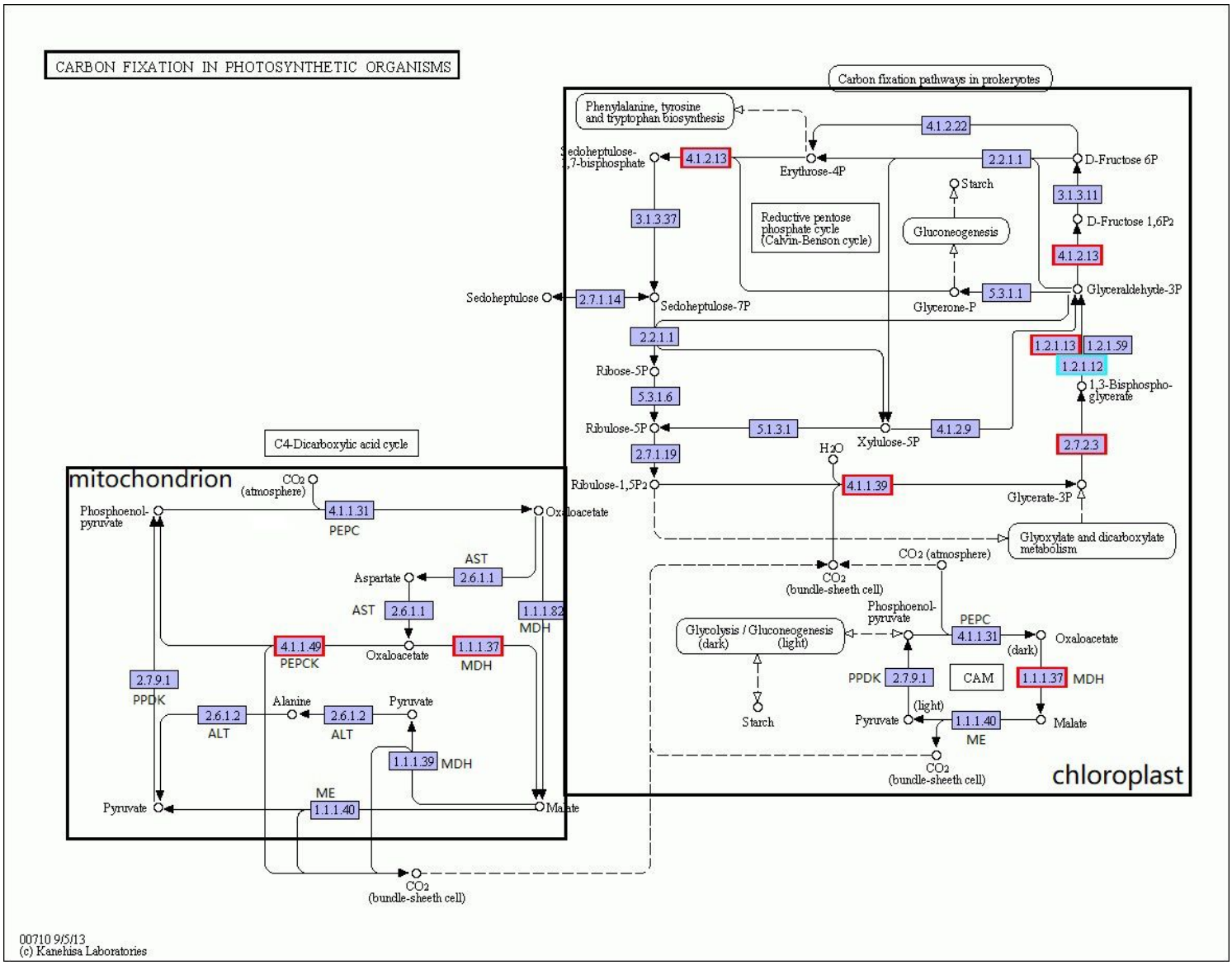

Figure 6

Overview of the putative biochemical CCM pathway in P. yezoensis.

Supplementary Files

This is a list of supplementary files associated with this preprint. Click to download.

- AF2figS1.tif
- Afile5TableS4.docx
- Afile4TableS3.docx
- Afile3TableS2.docx
- Afile1TableS1.docx